Visualizing the Motion of Graphene Nanodrums

Dejan Davidovikj,*[†] Jesse J. Slim,[†] Santiago J. Cartamil-Bueno,[†] Herre S. J. van der Zant,[†] Peter G. Steeneken,[†] and Warner J. Venstra*[†,‡]

[†]Kavli Institute of Nanoscience, Delft University of Technology, Lorentzweg 1, 2628 CJ, Delft, The Netherlands
[‡]Quantified Air, Lorentzweg 1, 2628 CJ, Delft, The Netherlands

S *Supporting Information*

ABSTRACT: Membranes of suspended two-dimensional materials show a large variability in mechanical properties, in part due to static and dynamic wrinkles. As a consequence, experiments typically show a multitude of nanomechanical resonance peaks, which make an unambiguous identification of the vibrational modes difficult. Here, we probe the motion of graphene nanodrum resonators with spatial resolution using a phase-sensitive interferometer. By simultaneously visualizing the local phase and amplitude of the driven motion, we show that unexplained spectral features represent split degenerate modes. When taking these into account, the resonance frequencies up to the eighth vibrational mode agree with theory. The corresponding displacement profiles, however, are remarkably different from theory, as small imperfections increasingly deform the nodal lines for the higher modes. The Brownian motion, which is used to calibrate the local displacement, exhibits a similar mode pattern. The experiments clarify the complicated dynamic behavior of suspended two-dimensional materials, which is crucial for reproducible fabrication and applications.

KEYWORDS: *Graphene, NEMS, interferometry, mode shape*
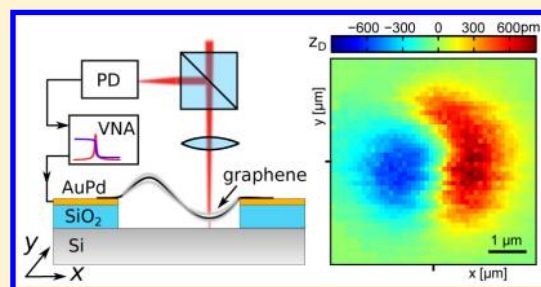
Nanomechanical devices from suspended graphene and other two-dimensional materials have received growing interest in the past few years,[1−4] and their application in sensitive pressure, gas, and mass sensors has been proposed.[5−11] Available techniques to study the mechanical properties of such membranes include quasistatic indentation[12,13] and dynamic response analyses in frequency- and time-domains.[1−3,14−16] These experimental studies show a large variability in the mechanical properties,[2,14,17] and to understand the intricate dynamic behavior of suspended graphene, it is necessary to detect its motion with spatial resolution. While initial experiments were done on structures with radial symmetry broken by design,[18−20] the local phase of the membrane motion was not measured in these cases, which makes identification of the mode difficult, especially for the higher modes and in the presence of small imperfections. Moreover, previous experiments did not measure absolute displacements, which makes the acquisition of quantitative displacement profiles of the fundamental and higher modes impossible.

Here, we visualize the motion of two-dimensional nanodrums with unprecedented resolution and sensitivity using a phase-sensitive scanning interferometer. The driven motion and the nondriven Brownian motion of a suspended few-layer graphene resonator vibrating at very high frequencies are detected up to the eighth vibrational mode. The phase information enables a reconstruction of the time-evolution of the displacement profile. In the radially symmetric nanodrum, we observe splitting of multiple degenerate modes as well as a

distortion of the mode structure. By visualizing the Brownian motion, the displacement profiles are calibrated in order to obtain spatially resolved displacement amplitudes. The spatially resolved measurements enable a detailed examination of the mode structure and provide a useful tool in the efforts toward reproducible fabrication of suspended two-dimensional materials.

Circular graphene nanodrums are fabricated by transferring exfoliated few-layer graphene on top of silicon substrates prepatterned with circular holes, as is described in the Methods section and in Supporting Information S1. Figure 1, panel a shows the graphene nanodrum of interest, with a diameter of 5 μm and a thickness of 5 nm as confirmed by Raman spectroscopy and atomic force microscopy (Figure 1b). The approximate mass of the moving part equals 230 fg. The flexural motion of the nanodrum is detected using an optical interferometer, which has been used previously in frequency- and time-domain studies of the nanomechanical properties of 2D-materials.[1,2,13,22,23] Figure 1, panel c shows the setup and a schematic cross-section of the graphene nanodrum. The drum is probed by a Helium−Neon laser, and the intensity variations caused by the interfering reflections from the moving membrane and the fixed silicon substrate underneath are detected with a photodiode, as described in more detail in Supporting Information S2.
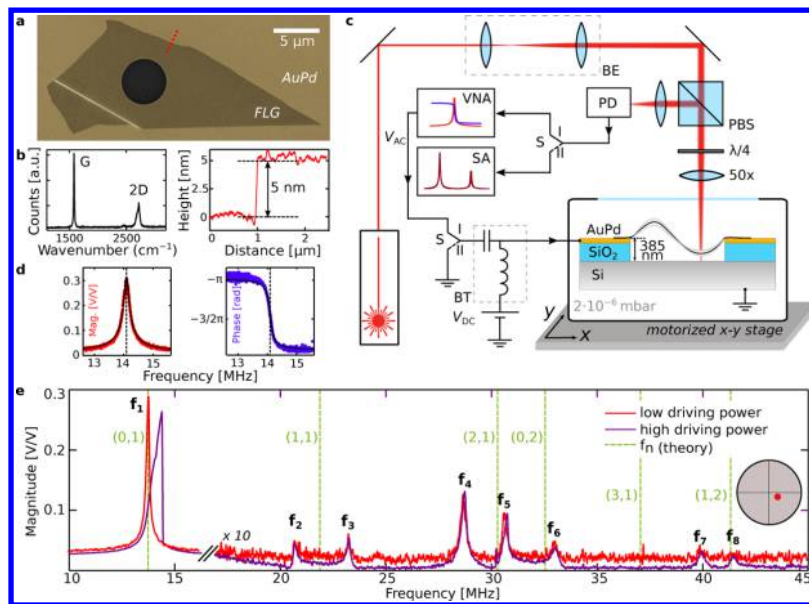
Figure 1. Scanning laser interferometry of graphene nanodrums. (a) Scanning electron microscope (SEM) image of the graphene nanodrum. (b) Raman spectrum (left) taken at the center of the drum; the relative height of the G and 2D peaks is characteristic of multilayer graphene. Atomic force microscope (AFM) trace (right) taken along the red dashed line from panel a, showing the flake thickness of 5 nm. (c) Interferometric displacement detection is accomplished by focusing a HeNe laser beam (λ = 632.8 nm) on the nanodrum while recording the interfering reflections from the graphene and the Si substrate underneath using a photodiode (PD). The sample is mounted on a motorized xy nanopositioning stage that scans the sample in a serpentine fashion, with a step size of 140 nm. BE, 3× beam expander; PBS, polarized beam splitter. Two measurement types can be selected using switch S: S = I engages a phase-sensitive vector network analyzer (VNA) measurement, while S = II is used to detect the Brownian motion of the nanodrum using a spectrum analyzer (SA). (d) VNA measurement (magnitude and phase) of the fundamental resonance mode, detected while probing at the center of the drum (black curves: fitted response). (e) VNA measurement showing the eight lowest resonance modes of the nanodrum when driven at $V_{ac,rms}$ = 2.2 mV (red) and $V_{ac,rms}$ = 8.9 mV (purple). Eight resonance peaks are detected, which are indexed f_1–f_8 starting at the fundamental mode (for clarity, the magnitude of modes 2−8 is scaled 10×). The dashed green lines mark the calculated frequencies for a circular tension-dominated membrane.[21]
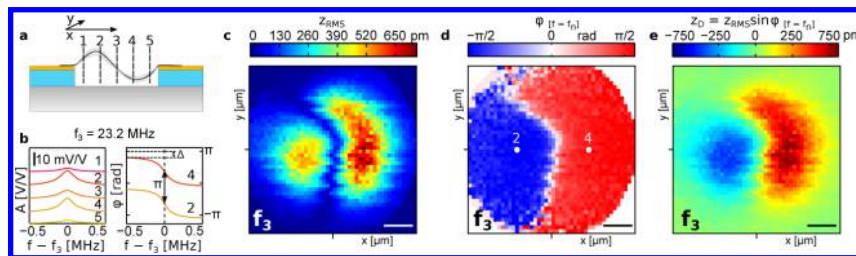

Figure 2. Spatially resolved measurements. (a) Individual frequency response lines taken at positions 1−5 using the VNA (S = 1) while applying a driving signal at f_3. (b) Recorded magnitude (left) and phase (right) response at f_3. A phase difference π indicates that on these locations the drum moves in opposite direction. (c) Root−mean−square displacement z_{RMS} of mode f_3, taken at a step size (x,y) of 140 nm. The diffraction-limited spot size of the probe laser is 1.3 μm, which causes some loss of spatial resolution. (d) Local phase response, ϕ_R, of the nanodrum, showing that two halves of the drum move in opposite directions. (e) Reconstructed displacement field map as obtained by $z_D = z_{RMS} \sin \phi$. Scale bars in panels c−e: 1 μm.

The sample can be moved in-plane using a motorized nanopositioning stage. Compared to a scanning mirror, moving the sample does not affect the intensity of the incident light such that the transduction gain of the setup remains constant. This makes a calibration of the displacements possible, as will be shown further. With a step size of 140 nm, the spectral response is measured at 1500 points spatially distributed across the suspended part of the drum, sufficient to visualize the displacements associated with higher vibration modes, which exhibit an increasing number of nodal lines.

Two measurement types can be selected by setting the switch S (see Figure 1c). When S = I, the complex response (magnitude and phase) to an electrostatic driving signal is measured using a vector network analyzer (VNA). When S = II, the driving signal is switched off, and the Brownian motion of the membrane is detected using a spectrum analyzer (SA). Figure 1, panel d shows the magnitude and phase response (S = I) at the fundamental resonance mode, which corresponds well to a harmonic oscillator. Figure 1, panel e shows the response of the drum at higher driving frequencies, taken at low (red curve) and high (black curve) driving voltages, when probing close to the center of the drum. At strong driving, a multitude of peaks is detected, which are labeled f_i, according to their position in the spectrum. The resonance frequencies calculated for a perfect circular membrane are also displayed.[24] The measured resonance frequencies are conspicuously different from the calculated ones, which raises the central question addressed in this work: which mode indices correspond to each of the observed resonance peaks?
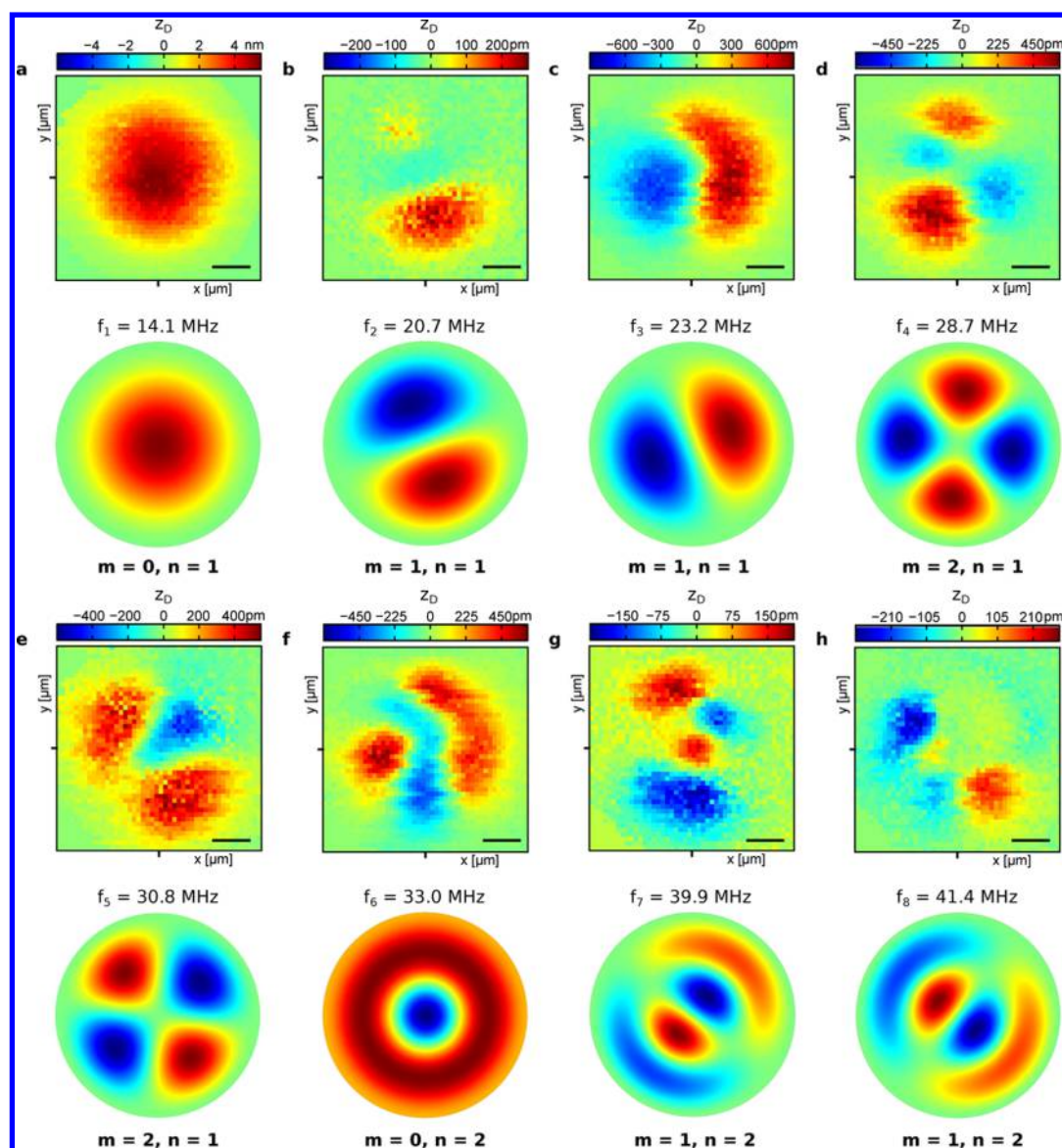
Figure 3. Visualizing resonant motion. (a−h) Top, experimental data; bottom, finite-element calculation. The modes predicted by the calculation are indexed by (m,n). Panels b and c show that the nanodrum hosts a split degenerate (1,1) mode, while also the (2,1) mode is split, as is shown in panels d and e. The displacement profile measured in panel f resembles a (0,2) mode, which is distorted due to an imperfection as discussed in the main text. Panels g and h reveal a degenerate (1,2) mode. Scale bars: 1 μm.

The motion of the graphene nanodrum is made visible using a phase-sensitive scanning interferometer. To demonstrate the technique, we set out by measuring the frequency response of mode 3 at five different positions on the drum, as illustrated in Figure 2, panel a. The amplitude and phase responses are fit to a harmonic oscillator function, and the fits are shown in Figure 2, panel b. From the responses, it is observed that while two halves of the drum move at a comparable amplitude, their phase differs by π. This indicates that at positions 2 and 4, the graphene moves in opposite direction, as is the case for a (1,1) mode.[24] Following this procedure, a more refined measurement is performed. Figure 2, panels c and d display on a color scale the fitted peak height, z_{RMS}, and phase responses ϕ at the resonance peak frequency, measured on a square grid with a spacing of 140 nm. The amplitude response reveals two antinodal points, which are separated by a nodal line, and the phase response shows that on either side of the nodal line the graphene moves in opposite direction. While for the (1,1)

mode this phase behavior appears trivial, we will show below that the phase information is a requisite to understand the motion of higher modes. Figure 2, panel e shows a snapshot colormap of the membrane movement, as obtained by $z_D = z_{RMS} \sin \phi$. A time-lapsed visualization of the motion over the oscillation period is provided in the Supporting Video.

In a similar way, the motion at the other resonance peaks of Figure 1, panel e is visualized. Figure 3, panels a−h show the mode shapes that correspond to $f_1 - f_8$, together with the theoretical shapes, which were obtained by finite-element calculations for a circular membrane. The fundamental mode was probed at a reduced driving voltage as to maintain a linear response as in Figure 1, panel e, red curve. The measurements show unambiguously that the peaks observed in the spectrum of Figure 1, panel e are the result of split degenerate modes (1,1), (1,2), and (2,1). The displacement profiles of modes 1−4 (Figure 3a−d) are in reasonable agreement with the theoretically calculated mode shapes. Other modes, however,

in particular the ones with higher indices (i.e., f_5, f_6, and f_8 as shown in Figure 3e–g), show a large discrepancy. Clearly, an imperfection is present whose influence on the location of the nodal lines grows with the mode index. Note that this imperfection is not visible in the SEM image of Figure 1, panel a, but has a large impact on the mode shapes. Table 1 summarizes the experimental and theoretical resonance frequencies and mode shapes and will be described further in the next section.

Table 1. Experimental and Theoretical Resonance Frequencies of the Graphene Nanodrum

	experiment		theory		
i	f_i [MHz]	f_i/f_0	f_i/f_0	(m, n)	shape
1	14.1	1	1	(0, 1)	
2	20.69	1.467	1.593	(1, 1)	
3	23.24	1.648			
4	28.73	2.038	2.135	(2, 1)	
5	30.75	2.181			
6	33	2.340	2.295	(0, 2)	
-	-	-	2.653	(3, 1)	
-	-	-			
7	39.93	2.832	2.917	(1, 2)	
8	41.41	2.937			

The above experiments illustrate in detail the mode structure of a driven graphene nanodrum, and it is interesting to compare these driven measurements with the displacements that are the result of thermal fluctuations. Compared to silicon carbide microdisk resonators, whose thermal motion was studied recently,[25] graphene nanodrums have a very low reflectivity and a 10−100-times lower mechanical Q-factor. Nevertheless, the present technique is sensitive enough to visualize their Brownian motion.

To study the Brownian motion, the switch is set to S = II to switch-off the driving signal and to record displacements with a spectrum analyzer. Figure 4, panel a shows an example of a thermal noise spectrum, taken close to the center of the drum. Three vibrational modes are observed that resemble the lowest three resonances of Figure 1, panel e, albeit at somewhat lower frequencies. The difference in frequency results from the absence of the electrostatic force: as $V_{dc} = 0$, no force is exerted on the graphene drum. Compared to the driven measurement, a part of the mechanical tension is released, which causes the resonance frequencies to tune to a lower value. Supporting Information S3 discusses the tuning of the resonance frequency as well as the optimization of the signal-to-noise ratio by adjusting V_{dc}. With the same step size as in the driven measurement, we map the first three mode shapes and plot the thermal RMS displacement as a function of position. Figure 4, panel b shows the Brownian motion of the fundamental (0,1) mode, and Figure 4, panels c and d show a splitting of the degenerate (1,1) mode, in close agreement with the amplitude map of the driven motion. Note that in the absence of a driving signal the phase is not measured as it diffuses within the measurement time.

For applications of suspended two-dimensional materials, it is important to quantify the displacements associated with the motion. The RMS displacement of a nanomechanical resonator can be obtained by measuring its Brownian motion.[26] From the power spectral density of the signal measured at the center of the drum, $S_{VV}(f) = S_{VV}^w + \alpha S_{zz}(f)$, the noise floor S_{VV}^w and the transduction factor α [V²/m²] are calculated. The thermal displacement noise spectral density of the fundamental mode at the drum center is given by

$$S_{zz}(f) = \frac{k_B T f_1}{2\pi^3 m_{\text{eff},1} Q_1 [(f^2 - f_1^2)^2 + (f_1 f / Q_1)^2]}$$

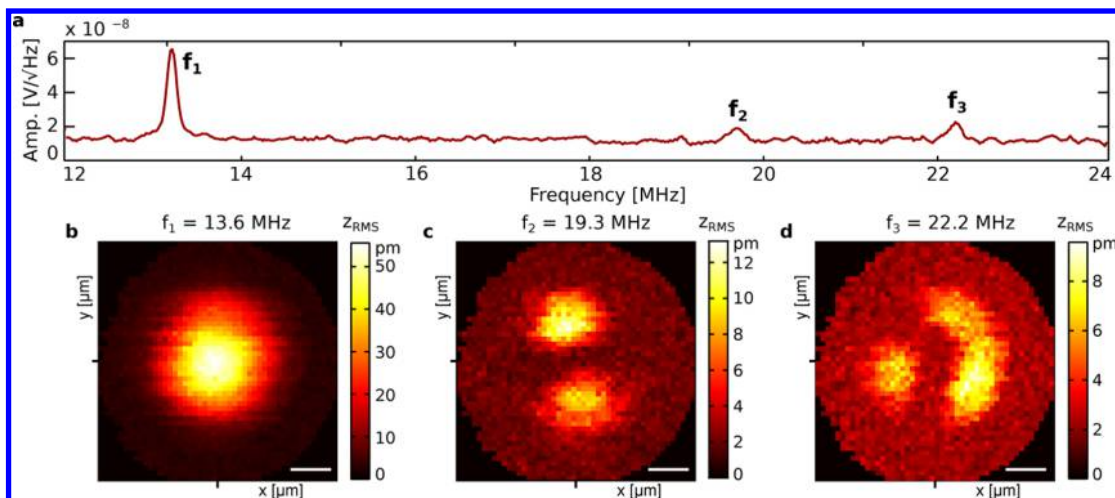**Figure 4.** Visualizing Brownian motion. (a) Spectrum analyzer measurements (S = II) taken without applying a driving signal ($V_{ac} = 0$) reveal three vibrational modes. (b–d) Spatial maps of the RMS Brownian displacements at each of the vibrational modes. The Brownian mode shapes correspond well with the ones observed when the drum is resonantly driven (Figure 3a–c). The slightly lower frequencies are the result of the absence of a dc-voltage $V_{dc} = 0$ V, which results in a lower mechanical tension in the drum, as discussed in Supporting Information S3.

where f_1 is the resonance frequency, Q_1 is the quality factor, and $m_{eff,1} = 0.2695 m_{total}$ its effective mass.[21] T equals the ambient temperature. Note that the effective temperature of the mode is up to a few K below the ambient temperature due to combined effects of laser heating and photothermal damping,[27] as discussed in detail in Supporting Information S4 and S5. Using an incident optical power of 0.8 mW, the noise floor equals $11 fm/\sqrt{Hz}$, which enables the detection of the three lowest resonance modes. The transduction factor equals $\alpha = 3.75 \times 10^{11}$ V^2/m^2, and using this number, all detected displacement signals in the experiments of Figures 3 and 4 are converted to absolute displacements and indicated in the respective color bars.

From the summary of the measurement results presented in Table 1, it becomes clear that the ratios of the higher harmonics to the fundamental mode, f_n/f_0, deviate from the theoretically expected frequencies for a membrane resonator.[28] Deviations range from 0.7% for mode f_8 to 8.6% for mode f_2. While the spatial maps show that the difference between the measured and theoretical mode shapes increases with the mode index, there is no obvious correlation between the differences in the resonance frequencies and the distortion of the mode shapes. For example, the mode shape of f_3 is in good agreement, while the mode shape of f_8 bears almost no resemblance to the theoretical calculation. Interestingly, comparing them in the frequency domain, f_8 differs by only 0.7% and f_3 by 3.3% from its theoretical value. Similarly, the frequency of f_6 is within 2% of the calculated value, while the corresponding shape is highly distorted due to a broken radial symmetry. Thus, the lower modes appear more robust against imperfections, possibly due to the lower number of nodal lines—a tendency that is confirmed by finite-element simulations provided in Supporting Information S6. These findings are of particular interest in the light of the recently proposed nanomechanical schemes to detect the *location and geometry* of adsorbed masses,[29,30] which rely on an accurate description of the mode shapes. In such schemes, the splitting of the degenerate modes, which is also observed in the Brownian motion and emerges from the structural imperfections in our experiments, could be used to provide such information about the adsorbed mass.

It is interesting to further investigate the origins of the mode-splitting and the progressive distortion of the mode structure for the higher modes. To this end, we map the local stiffness of the drum using peak-force AFM (measurement details provided in Supporting Information S6). The analysis reveals local inhomogeneities in the membrane that went unnoticed during optical and electron microscopy inspection. These may be the result of a uniaxial residual tension in the drum, introduced while "peeling-off" the graphene flake during the transfer to the substrate.[31] Similar effects were observed in other drums studied, which include a single-layer and a 13-layer graphene device (measurements are provided in Supporting Information S7), and it can thus be expected from this work that these are inherent to suspended two-dimensional materials fabricated by exfoliation and dry transfer. A finite-element calculation that takes this feature into account results in a better agreement between the predicted mode shapes and the measurements, as discussed in Supporting Information S6.

Besides the displacements on resonance described above, other parameters can be visualized with spatial resolution. For example, the local resonance frequency, the Q-factor, and the noise floor give a wealth of information about the device and the detector, such as the local temperature distribution in the device, and the local reflectivity of the substrate. These examples are discussed in more detail in Supporting Information S4. Spatially resolved measurements are a valuable tool to analyze the dynamic properties of two-dimensional materials and may be used to address open questions such as the origin of their low mechanical Q-factors[32,33] as well as to assess fabrication quality and reproducibility. These are essential to exploit opportunities that arise in new applications as hybrid nanoelectromechanical systems, which fuse excellent mechanical properties with exotic traits such as a negative thermal expansion coefficient and Poisson's ratio[34,35] and electromechanical[36,37] and optoelectronic couplings.[38]

In conclusion, we visualize the motion of micrometer-scale graphene drums vibrating at very high frequencies with a lateral resolution of 140 nm and a displacement resolution of $11 fm/\sqrt{(Hz)}$. The driven and nondriven thermal displacement profiles of the radially symmetric drum reveal the motion associated with nanomechanical resonance peaks up to the eighth vibrational mode. The spatial technique presented in this work complements the frequency- and time-domain techniques presently available and is crucial to obtain a complete description of the dynamic behavior of suspended two-dimensional materials.

Methods. The nanodrums were fabricated on a p-type silicon wafer with a 285 nm thick layer of thermal silicon oxide. First, the top electrodes, the circular cavities, and the bonding pads are patterned using e-beam lithography. A layer of Ti/AuPd (5/95 nm) is evaporated on top to provide a smooth and electrically conducting surface for the adhesion of graphene. After lift-of, metallic islands are fabricated, which serve as a hard mask during the subsequent reactive ion etching of SiO$_2$. The thickness of the metalization was chosen to obtain a cavity depth of 385 nm, which optimizes the responsivity of interferometric measurements at the wavelength of the probing laser ($\lambda = 632.8$ nm), as is described in detail in Supporting Information S2. In the final step, graphene flakes are mechanically exfoliated from natural crystals and deposited on top of the substrates using a dry transfer method.[31]

The suspended graphene drum is electrostatically driven by applying a voltage, $V_{dc} + V_{ac}$ to the AuPd pad while connecting the Si back-gate to ground. The dc-voltage tunes the static tension in the graphene flake, while the ac-voltage excites its resonant motion. The measurements of Figure 1, panel e are carried out with $V_{ac} = 2.2$ mV (red curve, linear response) and $V_{ac} = 8.9$ mV (black curve, nonlinear response). In both cases, a dc-bias voltage $V_{dc} = 3$ V is used to amplify the time-dependent actuation force via $F(t) \propto V_{dc}V_{ac} \sin(2\pi ft)$ and to electrostatically control the tension as to optimize the signal-to-noise ratio, as described in detail in Supporting Information S3. The xy-stage is actuated using NewFocus type 8301 picomotors with a type 8732 multiaxis driver. The xy-motion is calibrated by a software routine. All experiments are conducted at room temperature, at a pressure of $\sim 2 \times 10^{-6}$ mbar. The samples were kept inside the vacuum chamber for at least 48 h prior to the measurements to ensure that the pressure inside the cavity is equal to the pressure in the chamber.[5] All measurements were performed at an incident laser power of 0.8 mW.

■ ASSOCIATED CONTENT

Ⓢ Supporting Information

The Supporting Information is available free of charge on the ACS Publications website at DOI: 10.1021/acs.nano-lett.6b00477.

> Time-lapsed visualization of the motion over the oscillation period (MPG)
> Additional measurements on a single-layer graphene device and on a 13-layer graphene device, details on the device fabrication and optimization of the cavity depth, electrostatic tuning of the resonance frequency, finite element calculations, and an analysis of the laser-induced heating and photothermal damping (PDF)

■ AUTHOR INFORMATION

Corresponding Authors
*E-mail: d.davidovikj@tudelft.nl.
*E-mail: w.j.venstra@tudelft.nl.

Notes
The authors declare no competing financial interest.

■ ACKNOWLEDGMENTS

■ REFERENCES

(1) Bunch, J. S.; Van Der Zande, A. M.; Verbridge, S. S.; Frank, I. W.; Tanenbaum, D. M.; Parpia, J. M.; Craighead, H. G.; McEuen, P. L. *Science* **2007**, *315*, 490−493.

(2) Castellanos-Gomez, A.; van Leeuwen, R.; Buscema, M.; van der Zant, H. S. J.; Steele, G. A.; Venstra, W. J. *Adv. Mater.* **2013**, *25*, 6719−6723.

(3) Wang, Z.; Jia, H.; Zheng, X.; Yang, R.; Wang, Z.; Ye, G.; Chen, X.; Shan, J.; Feng, P. X.-L. *Nanoscale* **2015**, *7*, 877−884.

(4) Cartamil-Bueno, S. J.; Steeneken, P. G.; Tichelaar, F. D.; Navarro-Moratalla, E.; Venstra, W. J.; van Leeuwen, R.; Coronado, E.; van der Zant, H. S. J.; Steele, G. A.; Castellanos-Gomez, A. *Nano Res.* **2015**, *8*, 2842−2849.

(5) Bunch, J. S.; Verbridge, S. S.; Alden, J. S.; van der Zande, A. M.; Parpia, J. M.; Craighead, H. G.; McEuen, P. L. *Nano Lett.* **2008**, *8*, 2458−2462.

(6) Smith, A.; Vaziri, S.; Niklaus, F.; Fischer, A.; Sterner, M.; Delin, A.; Östling, M.; Lemme, M. *Solid-State Electron.* **2013**, *88*, 89−94.

(7) Koenig, S. P.; Wang, L.; Pellegrino, J.; Bunch, J. S. *Nat. Nanotechnol.* **2012**, *7*, 728−732.

(8) Wang, L.; Drahushuk, L. W.; Cantley, L.; Koenig, S. P.; Liu, X.; Pellegrino, J.; Strano, M. S.; Bunch, J. S. *Nat. Nanotechnol.* **2015**, *10*, 785−790.

(9) Jensen, K.; Kim, K.; Zettl, A. *Nat. Nanotechnol.* **2008**, *3*, 533−537.

(10) Sakhaee-Pour, A.; Ahmadian, M.; Vafai, A. *Solid State Commun.* **2008**, *145*, 168−172.

(11) Dolleman, R. J.; Davidovikj, D.; Cartamil-Bueno, S. J.; van der Zant, H. S. J.; Steeneken, P. G. *Nano Lett.* **2016**, *16*, 568−571.

(12) Poot, M.; van der Zant, H. S. J. *Appl. Phys. Lett.* **2008**, *92*, 063111.

(13) Nicholl, R. J.; Conley, H. J.; Lavrik, N. V.; Vlassiouk, I.; Puzyrev, Y. S.; Sreenivas, V. P.; Pantelides, S. T.; Bolotin, K. I. *Nat. Commun.* **2015**, *6*, 8789.

(14) van der Zande, A. M.; Barton, R. A.; Alden, J. S.; Ruiz-Vargas, C. S.; Whitney, W. S.; Pham, P. H. Q.; Park, J.; Parpia, J. M.; Craighead, H. G.; McEuen, P. L. *Nano Lett.* **2010**, *10*, 4869−4873.

(15) Eichler, A.; Moser, J.; Chaste, J.; Zdrojek, M.; Wilson-Rae, I.; Bachtold, A. *Nat. Nanotechnol.* **2011**, *6*, 339−342.

(16) van Leeuwen, R.; Castellanos-Gomez, A.; Steele, G. A.; van der Zant, H. S. J.; Venstra, W. J. *Appl. Phys. Lett.* **2014**, *105*, 041911.

(17) Barton, R. A.; Ilic, B.; van der Zande, A. M.; Whitney, W. S.; McEuen, P. L.; Parpia, J. M.; Craighead, H. G. *Nano Lett.* **2011**, *11*, 1232−1236.

(18) Garcia-Sanchez, D.; van der Zande, A. M.; Paulo, A. S.; Lassagne, B.; McEuen, P. L.; Bachtold, A. *Nano Lett.* **2008**, *8*, 1399−1403.

(19) Wang, Z.; Lee, J.; He, K.; Shan, J.; Feng, P. X.-L. *Sci. Rep.* **2014**, *4*, 3919.

(20) Liu, C.-H.; Kim, I. S.; Lauhon, L. J. *Nano Lett.* **2015**, *15*, 6727−6731.

(21) Hauer, B.; Doolin, C.; Beach, K.; Davis, J. *Ann. Phys.* **2013**, *339*, 181−207.

(22) Azak, N. O.; Shagam, M. Y.; Karabacak, D. M.; Ekinci, K. L.; Kim, D. H.; Jang, D. Y. *Appl. Phys. Lett.* **2007**, *91*, 093112.

(23) Lee, J.; Wang, Z.; He, K.; Shan, J.; Feng, P. X.-L. *ACS Nano* **2013**, *7*, 6086−6091.

(24) In a circular membrane, the mode-shapes are labelled as (*m,n*), where *m* refers to the number of nodal diameters and *n* to the number of nodal circles.

(25) Wang, Z.; Lee, J.; Feng, P. X.-L. *Nat. Commun.* **2014**, *5*, 5158.

(26) Li, M.; Tang, H. X.; Roukes, M. L. *Nat. Nanotechnol.* **2007**, *2*, 114−120.

(27) Barton, R. A.; Storch, I. R.; Adiga, V. P.; Sakakibara, R.; Cipriany, B. R.; Ilic, B.; Wang, S. P.; Ong, P.; McEuen, P. L.; Parpia, J. M.; Craighead, H. G. *Nano Lett.* **2012**, *12*, 4681−4686.

(28) The motion of mode (3,1), with an expected resonance at 37.4 MHz, is not detected. A possible explanation is that the nodal lines in this device are spaced close to the diffraction limit, resulting in a low displacement contrast.

(29) Dohn, S.; Sandberg, R.; Svendsen, W.; Boisen, A. *Appl. Phys. Lett.* **2005**, *86*, 233501.

(30) Hanay, M. S.; Kelber, S. I.; O'Connell, C. D.; Mulvaney, P.; Sader, J. E.; Roukes, M. L. *Nat. Nanotechnol.* **2015**, *10*, 339−344.

(31) Castellanos-Gomez, A.; Buscema, M.; Molenaar, R.; Singh, V.; Janssen, L.; van der Zant, H. S. J.; Steele, G. A. *2D Mater.* **2014**, *1*, 011002.

(32) Helgee, E. E.; Isacsson, A. *Phys. Rev. B: Condens. Matter Mater. Phys.* **2014**, *90*, 045416.

(33) Kramer, E.; Van Dorp, D. J. J.; Van Leeuwen, R.; Venstra, W. J. *Appl. Phys. Lett.* **2015**, *107*, 091903.

(34) Yoon, D.; Son, Y.-W.; Cheong, H. *Nano Lett.* **2011**, *11*, 3227−3231.

(35) Jiang, J.-W.; Park, H. S. *Nat. Commun.* **2014**, *5*, 4727.

(36) Duerloo, K.-A. N.; Reed, E. J. *Nano Lett.* **2013**, *13*, 1681−1686.

(37) Wu, W.; Wang, L.; Li, Y.; Zhang, F.; Lin, L.; Niu, S.; Chenet, D.; Zhang, X.; Hao, Y.; Heinz, T. F.; et al. *Nature* **2014**, *514*, 470−474.

(38) Mak, K. F.; Lee, C.; Hone, J.; Shan, J.; Heinz, T. F. *Phys. Rev. Lett.* **2010**, *105*, 136805.